

Photon-induced jet production at future lepton colliders

Thomas Gehrmann and Peter Meinzinger

Physik-Institut, Universität Zürich, Winterthurerstrasse 190, CH-8057 Zürich, Switzerland

E-mail: thomas.gehrmann@uzh.ch, peter.meinzinger@uzh.ch

ABSTRACT: The production of hadronic final states in electron-positron or electron-hadron collisions is induced predominantly by quasi-real photons that were emitted off incoming leptons. In these processes, the photon either enters directly or through its resolved parton content, which is at present only loosely constrained by experimental data. We perform a detailed phenomenological study of photon-induced jet production processes in high-energy e^+e^- collisions, investigating in particular their potential to assess contributions from the resolved photon structure.

KEYWORDS: QCD, lepton-lepton collider, photon

Contents

1	Introduction	1
2	Setup for photon-lepton scattering	2
3	Results	4
4	Conclusion	11

1 Introduction

The interaction of quasi-real photons with other particles at high energies consists of two components [1,2]: a direct process, where the photon directly participates in the interaction, and a resolved process, where the photon splits up into a collinear cluster of particles prior to the interaction. For hadronic final states, in particular the primary splitting of the photon into a quark-antiquark pair and its subsequent partonic evolution are of relevance. These are described by an inhomogeneous variant [3] of the DGLAP evolution equations [4,5].

The description of the resolved process thus involves parton distributions (PDFs) of the photon, which describe the probabilities of finding partons with specific momentum fractions ξ at a resolution scale μ^2 inside the photon. These photon PDFs obey evolution equations [3] in μ^2 with non-perturbative initial conditions. These initial conditions are poorly constrained by data from e^+e^- and γp collisions, and are often modelled assuming so-called vector meson dominance (VMD) models [6–8] which describe the content of the photon as a superposition of light vector mesons.

An improved knowledge on the photon PDFs is crucial to improve the accuracy of predictions for hadronic final states in e^+e^- and ep collisions at high energies, which both receive substantial contributions from initial states with quasi-real photons. In the light of future high-energy e^+e^- colliders currently being discussed (FCC [9], CEPC [10], ILC [11]) and of the upcoming BNL Electron-Ion Collider (EIC, [12]), these predictions will become crucial both for physics studies and for background predictions to other processes under consideration that yield hadronic final states.

Currently available parametrizations [13–17] of the photon PDFs rely on fits to e^+e^- and γp data in combination with VMD models. Lacking recent data on these processes, no updates or refinements on the photon PDFs have been performed for nearly three decades. An overview on the status of data and theory relevant to photon PDFs can be found in [18].

In this article, we investigate the reach and sensitivity of future measurements on hadronic final states resulting from $e\gamma$ -initiated processes in e^+e^- collisions, in particular in view of probing the resolved photon contributions. In Section 2, we describe the simulation framework used in our study. The main results are discussed in Section 3, followed by a summary of our main findings in Section 4.

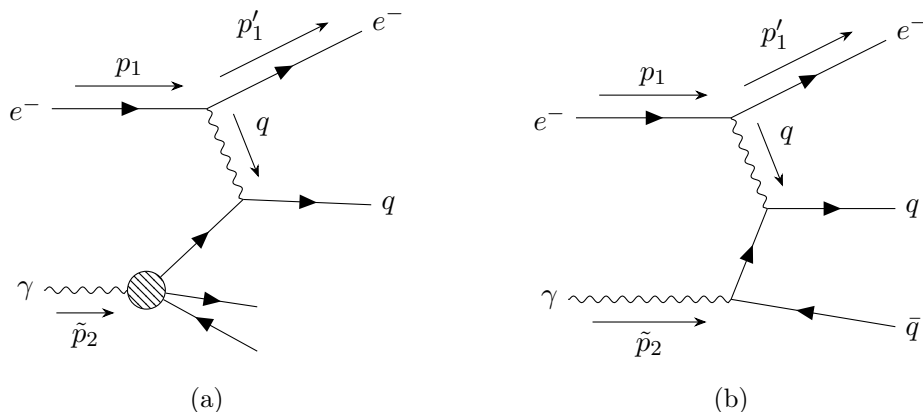


Figure 1: Examples of diagrams contributing to deep-inelastic scattering of an electron on a collinear quasi-real photon. (a) The photon can be resolved and interact hadron-like. (b) The direct contribution contributes at the level of two out-going partons.

2 Setup for photon-lepton scattering

We consider e^-e^+ beams with beam energies of 125 GeV using a pre-release version of SHERPA 3.1 [19] for the simulation of the process

$$e^-(p_1) + e^+(p_2) \xrightarrow{e^- \gamma} e^-(p'_1) + e^+(p'_2) + X \quad (2.1)$$

where X denotes any hadronic final state. The process is considered analogously to deep inelastic scattering (DIS), i.e. one lepton emits a quasi-collinear photon while the other one scatters at a large angle with that photon. The flux of quasi-real photons is calculated in the Weizsäcker-Williams approximation [20–22]

$$f_{\gamma/e^-}(z) = \frac{\alpha_{\text{em}}}{2\pi} \frac{dz}{z} \left[(1 + (1-z)^2) \log \left(\frac{Q_{\text{max}}^2}{Q_{\text{min}}^2} \right) - 2m_e^2 z^2 \left(\frac{1}{Q_{\text{min}}^2} - \frac{1}{Q_{\text{max}}^2} \right) \right] \quad (2.2)$$

with an assumed maximum virtuality of $Q_{\text{max}}^2 = 4 \text{ GeV}^2$ and with the minimum virtuality given by $Q_{\text{min}}^2 = \frac{m_e^2 z^2}{1-z}$.

The total cross-section for jet production through quasi-real photons is then the sum of two types of contributions: (i) direct contribution, i.e. $e\gamma \rightarrow ejj$, and (ii) the resolved contribution where the photon behaves hadron-like by resolving a parton p , i.e. $ep \rightarrow ej$. We show exemplary diagrams for both contributions in Fig. 1. In our computation, the hadron-like component is given by the SAS1M photon PDF [16]. At higher orders in perturbation theory, mass factorization and parton evolution [3] result in a mixing between both contributions, which can however still be assigned uniquely according to the underlying parton-level subprocesses.

Summing over the direct- and resolved-photon contributions, one has to make sure to coherently add these. While at lowest order, the resolved photon contributes at the level of $e^-p \rightarrow e^-j$, the direct photon only enters at the next multiplicity, i.e. $e^- \gamma \rightarrow e^-jj$, at the matrix-element level.

This issue can be overcome by employing merging to coherently add resolved and direct channels. Multi-leg merging creates inclusive samples from matrix-elements of different multiplicities while still allowing for resummation through parton showers in the relevant regions of phase space. This is achieved by phase-space slicing using a jet criterion that separates soft and hard regions, where the latter are described by matrix elements and the former by the parton shower. Here we adopt the MEPS@LO prescription [23, 24].

In this study, the merging of the resolved (pure QCD) channels is straightforward and follows previous studies [25]. To merge the direct channels, however, we have to consider a democratic QCD+QED evolution to allow for a clustering of the $\gamma \rightarrow q\bar{q}$ vertex [26]. Additionally, we have to enforce a clustering down to a $2 \rightarrow 2$ process such that the available phase space is filled and a coherent addition to the resolved channels is achieved. These contributions amount to the inclusion of the so-called anomalous components of the photon, which are part of the PDF evolution encapsulated in terms proportional to the $P_{\gamma q}$ DGLAP splitting kernel.

We calculate events with up to three jets at LO,

$$\begin{aligned} e^-e^+ &\xrightarrow{\rightarrow e^- \gamma} e^-jj + 0, 1j \quad \oplus \\ e^-e^+ &\xrightarrow{\rightarrow e^- \gamma \rightarrow e^- p} e^-j + 0, 1, 2j \end{aligned} \quad (2.3)$$

and the merging scale Q_{cut} is set dynamically depending on the virtuality [25], as

$$Q_{\text{cut}} = \frac{\bar{Q}_{\text{cut}}}{\sqrt{1 + \frac{\bar{Q}_{\text{cut}}^2}{S_{\text{DIS}}Q^2}}} \quad (2.4)$$

with $\bar{Q}_{\text{cut}} = 10$ GeV and $S_{\text{DIS}} = 1$. The factorisation and renormalisation scale are set according to $\mu_R^2 = \mu_F^2 = Q^2/4$ for $2 \rightarrow 2$ core processes and $\mu_R^2 = \mu_F^2 = (Q^2 + H_T^2)/4$ for higher multiplicities, where H_T is the scalar sum of the transverse momentum of partons in the final state.

The strong coupling is set to $\alpha_S(M_Z) = 0.118$ with 4-loop running and electroweak parameters are set using the G_μ scheme. We compute tree-level matrix elements with COMIX [27] and utilize CSSHOWER [28] and AHADIC [29] for parton-showering and hadron fragmentation, respectively. The factorisation and renormalisation scales are varied by factors of 2 to estimate missing higher-order corrections.

Events are then analysed using an interface to RIVET [30] by imposing a cut on both the virtuality Q^2 and the inelasticity y as computed with respect to the scattered electron, which is determined as the electron with the highest transverse energy. The computation follows in analogy to HERA analyses with the small-angle outgoing lepton taking the role of the hadron. In our setup, we choose the scattered lepton to be the electron, travelling in the $+z$ direction, and the photon being emitted by the positron, going in the $-z$ direction. The results generalize trivially to the opposite case.

The assumed detector acceptance is $|\eta| < 3$ and events are required to fulfill $Q^2 > 16$ GeV² and $0.1 < y < 0.9$, based on similar cuts from DIS analyses at HERA. Unless stated explicitly, we do also apply the $|\eta| < 3$ cut on the forward rapidity of the out-going

lepton. Jets are clustered with the anti- k_T algorithm with radius $R = 1.0$ and a requirement of $p_T > 5$ GeV. Variations of $0.4 < R < 1.0$ do not affect our findings below.

3 Results

The kinematical reach of the measurement is illustrated by the distributions in virtuality Q^2 and x_γ . These are defined as

$$Q^2 = -q^2 \quad \text{and} \quad x_\gamma = \frac{Q^2}{Q^2 + W^2} . \quad (3.1)$$

We additionally define the momentum ratio with respect to the incoming lepton, x , in analogy to the Bjorken variable, and the ratio z as

$$x = \frac{-q^2}{2q \cdot p_2} \quad \text{and} \quad z = \frac{x}{x_\gamma} . \quad (3.2)$$

It should be noted that both x and x_γ use definitions which in normal DIS settings would be equivalent, but in this context yield different interpretations. The definition of x is with respect to the incoming positron that radiates the quasi-real photon. The definition of x_γ , however, uses the mass of the hadronic final state, W , and is hence a ratio with respect to the underlying $e\gamma$ kinematics. Therefore, the ratio z can be interpreted as the momentum fraction of the lepton taken by the photon.

We first study the sensitivity to this process by considering the impact of the forward acceptance of the detector and by separating the direct and resolved components. Even though the distinction into these two components cannot be maintained strictly at higher orders, it is still informative and allows conclusions on the resulting impact on photon PDF fits.

In Fig. 2 it can be seen that indeed the resolved component is dominating the total cross-section, underlining the potential to fit the non-perturbative parton content of the photon. However, the forward acceptance of the scattered lepton is the limiting factor in the small- Q^2 and small- x_γ region, severely constraining the availability of data in that region. The lepton rapidity cut sets in quite sharply at around $Q^2 \simeq 12$ GeV² and $x_\gamma \simeq 0.8$, and leads to a suppression of the distributions by 90% in x_γ and by 99% in Q^2 . Towards larger values of Q^2 and x_γ , the contribution from the direct component increases gradually, becoming dominant in the region $Q^2 > 4 \cdot 10^3$ GeV² and up to 15% in the limit $x_\gamma \rightarrow 1$. The distribution of the mass of the hadronic final state is again largely dominated by the resolved component. However, it distinctly shows a Z^0 peak in the direct channels, above which these channels dominate. This peak is also visible in the z distribution, which marks the threshold for the $\gamma e \rightarrow Z^0 e \rightarrow jj e$ configuration. In terms of forward acceptance, we also observe a depletion of the signal for values of $W^2 < 10^4$ GeV² and $z < 0.4$ to about 20%.

We present leading-jet transverse momentum and jet multiplicity as complementary observables in Fig. 3, displayed for both the laboratory frame and the Breit frame which is usually chosen for analyses of deep-inelastic scattering. It is defined as the frame in which

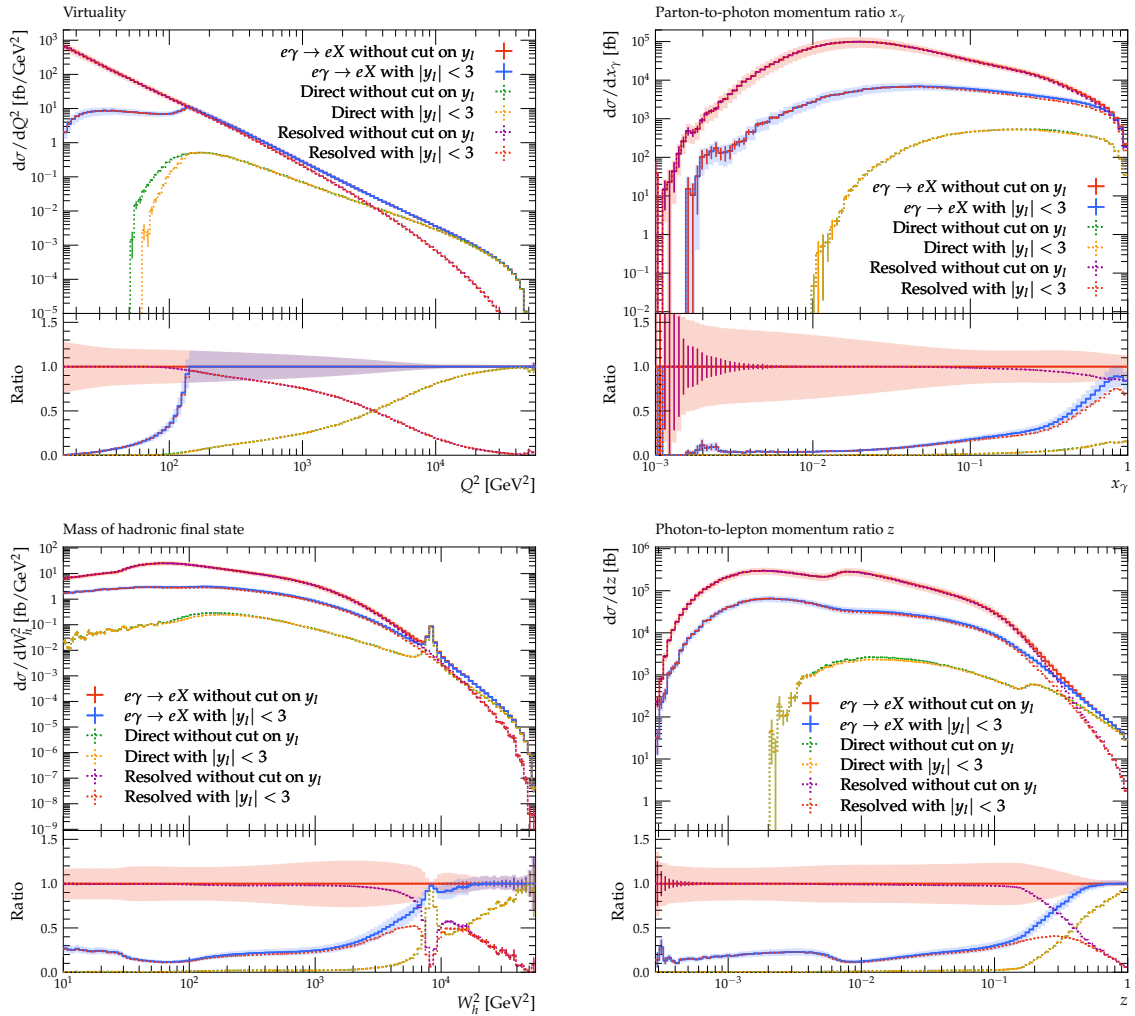


Figure 2: Distributions in virtuality Q^2 (top left), parton-to-photon momentum ratio x_γ (top right), hadronic mass W_h^2 (bottom left) and photon-to-lepton momentum ratio z (bottom right) for $e\gamma \rightarrow eX$, with and without cut on the rapidity of the out-going lepton, and separating the direct and resolved contributions to the cross-section.

the virtual photon acquires a four-momentum $q = (0, 0, 0, Q)$ and it can hence be fully determined by measuring the outgoing lepton. Its advantage is the natural separation into a hadronic and a leptonic hemisphere of the event.

In the Breit frame, the direct component is enhanced over the resolved one. This is a consequence of the fact that the resolved Born-level scattering process $eq \rightarrow eq$ results in a jet at finite transverse momentum only in the laboratory frame. Any jets in the Breit frame are a result of additional emissions, either from the parton-shower or from higher-multiplicity corrections in the hard matrix element. In contrast, the direct Born-level scattering process $e\gamma \rightarrow eq\bar{q}$ yields two-jet final states both in the laboratory and the Breit frame.

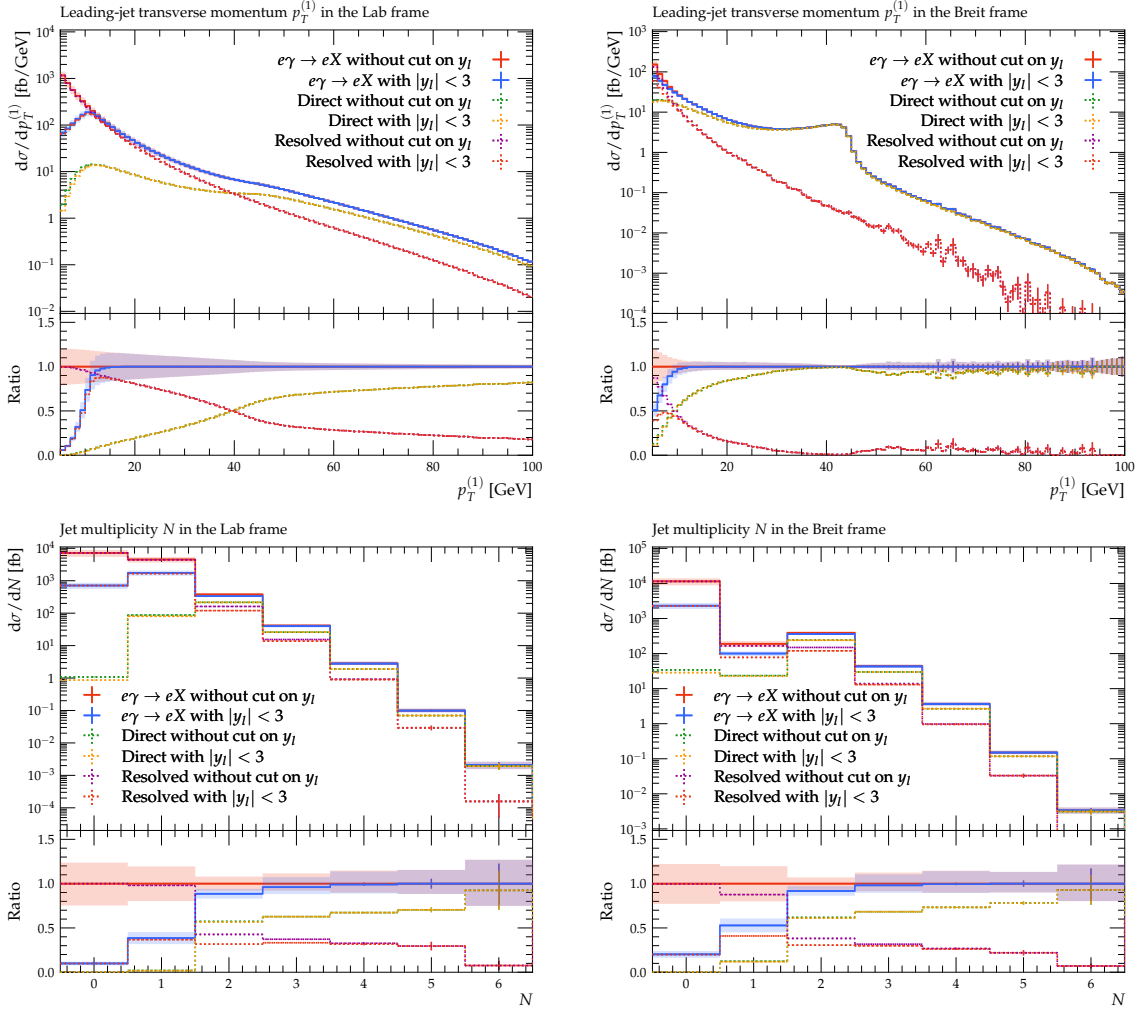


Figure 3: Distributions in leading jet transverse momentum $p_T^{(1)}$ (top row) and jet multiplicity N (bottom row) in the laboratory (left column) and Breit frame (right column) for $e\gamma \rightarrow eX$, with and without cut on the rapidity of the out-going lepton, and separating the direct and resolved contributions to the cross-section.

Consequently, the $N = 1$ jet fraction is lower by almost two orders of magnitude in the Breit frame (where it is comparable to the $N = 2$ jet fraction) than in the laboratory frame, and the normalization of the leading-jet transverse momentum distribution is suppressed by a similar factor. Moreover, the resolved component yields a sizable contribution in the Breit frame only for low jet transverse momenta $p_T < 10$ GeV. The forward rapidity cut affects the p_T distributions below 10 GeV and the multiplicity for $N \leq 1$ in both frames. From these observations, we conclude that jet cross sections in the Breit frame are not suitable for a study of the non-perturbative component of photon PDF, where the focus is on the resolved component.

Turning to jet clustering in the laboratory frame in the left-hand column in Fig. 3,

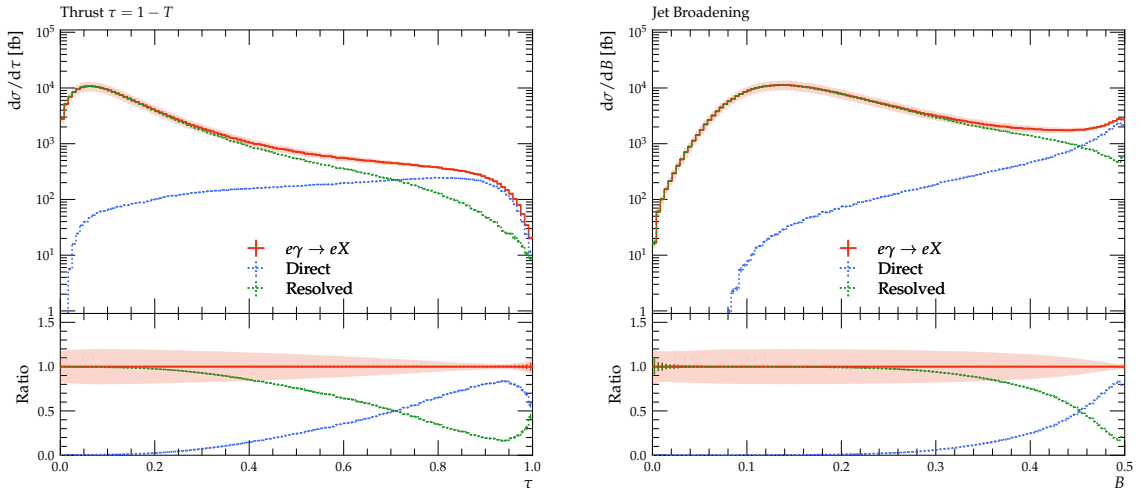


Figure 4: Event shape distributions in the variables thrust $\tau = 1 - T$ (left) and jet broadening B (right) for $e\gamma \rightarrow eX$, separating the direct and resolved contributions to the cross-section.

we see that 0- and 1-jet configurations dominate. In fact, the latter yields the highest cross-section once the forward acceptance of the lepton is taken into account. Comparing resolved and direct contributions, we can see that the latter starts to dominate in regions of high jet transverse momenta, $p_T > 40$ GeV, and high multiplicities, $N > 2$.

Event shape distributions provide an alternative to jet cross sections, offering access to a variety of hadronic final state characteristics. In the Breit frame in lepton-hadron scattering, event shape variables can be defined in close analogy to electron-positron annihilation. Consequently, event shape studies are usually performed in the Breit frame.

We focus on two commonly used event shape variables, thrust and jet broadening, which are both defined with respect to the axis of the exchanged boson as

$$\tau = 1 - T = 1 - \frac{\sum_h |p_{z,h}|}{\sum_h |\vec{p}_h|} \quad \text{and} \quad B = \frac{\sum_h |p_{\perp,h}|}{2 \sum_h |\vec{p}_h|}. \quad (3.3)$$

All momenta are evaluated in the Breit frame and the definitions follow an analysis by the H1 collaboration [31] of event shapes in electron-proton collisions at DESY HERA. By defining event shape variables relative to the boson axis, the event-shape distributions favour configurations where all hadronic activity is collimated along the z -axis in the Breit frame (as opposed to a principal back-to-back axis in electron-positron annihilation), thereby probing information that is highly complementary to jet distributions in the Breit frame, which require objects with larger transverse momenta.

This feature can be seen very clearly in the thrust and jet broadening distributions in Fig. 4. For the bulk of the phase space, the resolved channels yield the dominant contribution to the event shape distributions. The direct component yields significant contributions only towards the kinematical edges $\tau \rightarrow 1$ or $B \rightarrow 0.5$, which correspond to events with large transverse momenta in the Breit frame. Thrust and jet broadening may

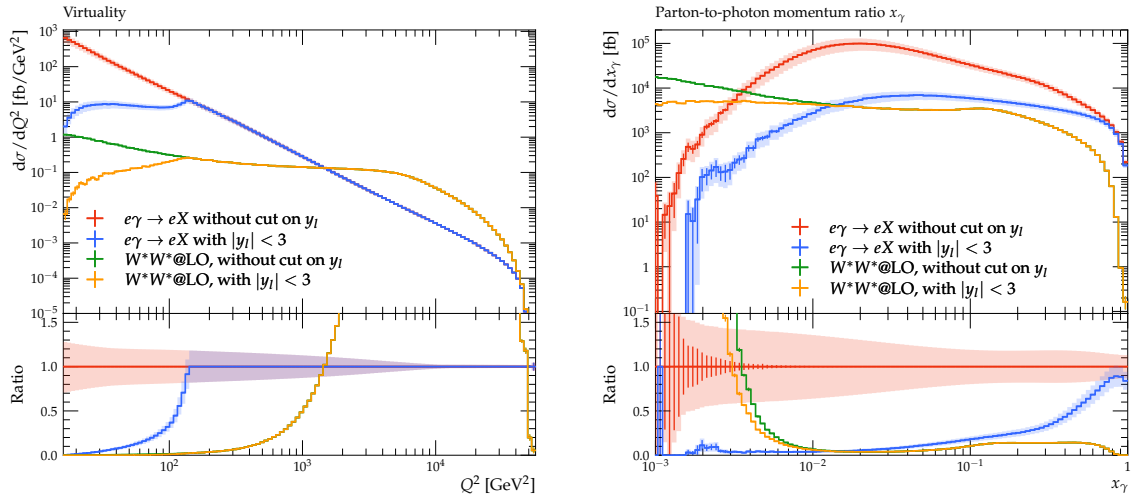


Figure 5: Distributions in virtuality Q^2 (left) and Bjorken variable x_γ (right), for the $e\gamma \rightarrow eX$ and $e^+e^- \rightarrow W^*_{\rightarrow l\bar{\nu}}W^*_{\rightarrow jj}$ processes, with and without cut on the rapidity of the out-going lepton.

thus be well-suited observables to separate resolved and direct contributions in $e\gamma$ collisions, suggesting a boundary around $\tau \approx 0.72$ and $B \approx 0.45$.

The final-state signature of the $e\gamma \rightarrow e$ +hadrons process at e^+e^- colliders consists of a single identified lepton plus final-state hadronic activity. A similar final-state signature can be produced through W -boson pair production $e^+e^- \rightarrow W^*W^* \rightarrow l\bar{\nu}jj$ as the neutrino is not detected. To arrive at predictions for this background, we again use SHERPA with an analogous setup as described in Sec. 2, but calculating $e^-e^+ \rightarrow e^-\bar{\nu}jj$ at leading order.

In Fig. 5, we compare the two processes with and without cuts on the forward acceptance of the lepton. We observe that the background of W pair production dominates the event rates for high values of Q^2 , starting at around $Q^2 \simeq 1.5 \cdot 10^3 \text{ GeV}^2$. In x_γ , the W pair background is negligible for $x_\gamma > 4 \cdot 10^{-3}$ as long as forward leptons are detected. Once a cut on this acceptance is included, the background contributes a significant fraction to the cross-section for $x_\gamma \lesssim 0.1$ and then becoming dominant for values of $x_\gamma < 10^{-2}$.

To identify potential ways of discrimination between the two processes, we investigate several kinematical distributions in Fig. 6: missing transverse momentum $p_{T,\text{miss}}$, lepton rapidity y_l , leading-jet pseudorapidity $\eta^{(1)}$ and jet multiplicity N in the laboratory frame. We observe that the differential cross-section of the lepton-photon scattering increases towards higher rapidities of the scattered lepton, whereas the W pair production drops off in that region of phase space. A cut on the lepton rapidity due to limited forward detector acceptance will thus mainly diminish the signal process, while leaving the background largely unaffected. The missing transverse momentum peaks as expected at around the W mass in the W pair production and at small values for the lepton-photon scattering, making this variable a potential separator between signal and background.

The pseudorapidity distribution of the leading jet is remarkably different for both pro-

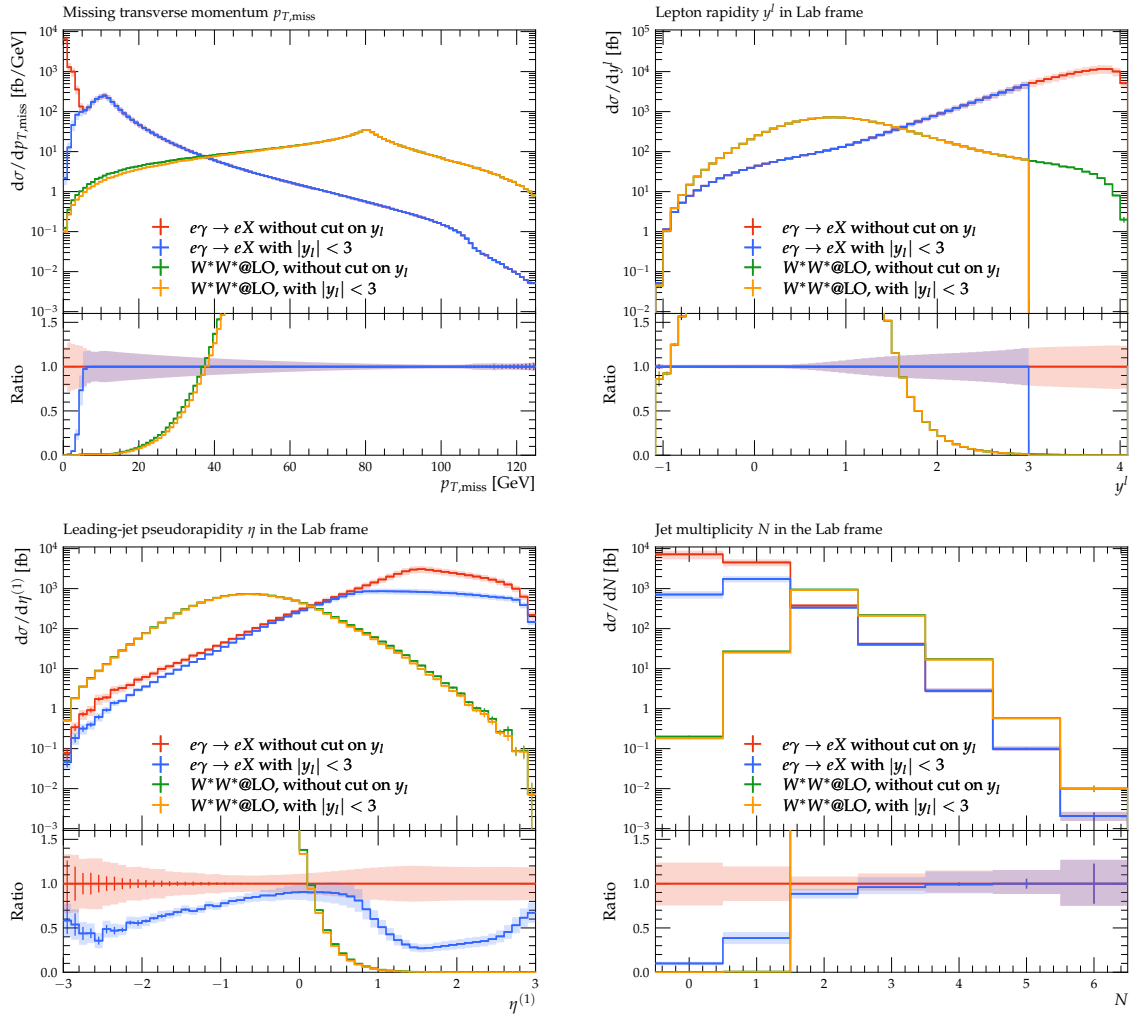


Figure 6: Distributions in missing transverse momentum $p_{T,\text{miss}}$ (top left), lepton rapidity y_l (top right), leading-jet pseudorapidity $\eta^{(1)}$ (bottom left) and jet multiplicity N (bottom right) in the laboratory frame for the $e\gamma \rightarrow eX$ and $e^+e^- \rightarrow W^*_{\rightarrow l\bar{\nu}}W^*_{\rightarrow jj}$ processes, with and without cut on the rapidity of the out-going lepton.

cesses. Here, we recall that the forward rapidity direction is determined by the electron beam, and that only final states with identified electrons are considered. The $\eta^{(1)}$ distribution is peaked in the forward region, corresponding to the direction of the incoming electron, while the W -pair production yields final states with leading jets preferably in the backward direction, resulting from the charge and spin correlations in the underlying Born process. Finally, another potential discriminator is the jet multiplicity in the laboratory frame, where the $e\gamma \rightarrow \text{hadrons}$ yields predominantly zero-jet and one-jet final states, while W -boson pair production in the semi-leptonic decay mode produces two-jet final states.

Based on these observations, we suggest three different cuts, which aim at improving the signal-to-background ratio for a study of the partonic content of the photon from e +hadrons

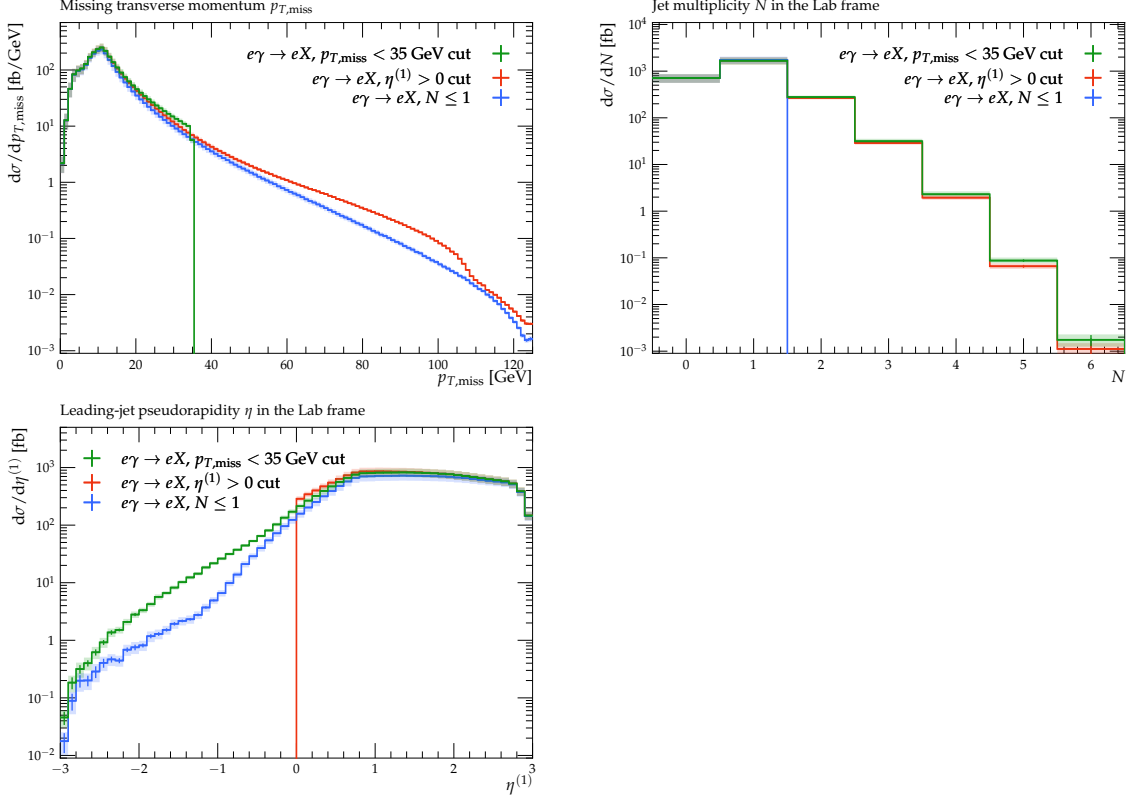


Figure 7: Distributions of missing transverse momentum $p_{T,\text{miss}}$ (left), jet multiplicity N (middle) and leading-jet pseudorapidity $\eta^{(1)}$ (right) for $e\gamma \rightarrow eX$. We compare different cuts to suppress the background from $e^+e^- \rightarrow W_{\rightarrow l\bar{\nu}}^* W_{\rightarrow jj}^*$, cutting on either $\eta^{(1)} > 0$, $p_{T,\text{miss}} < 35$ GeV or $N = 1$.

final states. These are either of the following

$$N_{\text{jets}} \leq 1 \quad \text{or} \quad \eta^{(1)} > 0 \quad \text{or} \quad p_{T,\text{miss}} < 35 \text{ GeV} \quad (3.4)$$

We compare the effect of these cuts in Fig. 7 in the respective distributions and observe them to be largely orthogonal to each other, i.e. cutting out completely separate parts of the phase space.

The effect of the different cuts on the distributions in Q^2 and in x_γ is illustrated in Fig. 8 for the signal and background processes. It can be seen that the cut on the jet multiplicity achieves the best enhancement of the lepton-photon scattering over the W -pair background, however, even in that case the latter dominates for high Q^2 . The cuts on leading jet pseudorapidity and $p_{T,\text{miss}}$ are less performant in the regions of large Q^2 , with the latter cut leading even to a complete suppression of the signal in this kinematical endpoint region. Similarly, the $N \leq 1$ cut achieves the best reduction of the boson-pair background for small values of x_γ , extending the range of a signal-to-background ratio above unity towards a value of $4 \cdot 10^{-3}$. As intended, neither of the cuts has significant impact in the region of small Q^2 and they lead only to a small reduction in the reach of small

x_γ . As none of the cuts is able to efficiently suppress the gauge-boson pair background in the large- Q^2 region, which is furthermore affected by large contributions from the direct channels, this region will be difficult to fully exploit for photon PDF fits.

4 Conclusion

In this study, we considered jet production through lepton-photon scattering at a future lepton collider. In high-energy collisions the photon exhibits an intricate partonic structure described by parton distribution functions. Measurements of lepton-photon scattering, in analogy to deep inelastic scattering, can be considered the signal processes to determine these distributions.

We indeed found that jet production at moderate momentum transfer Q^2 is particularly sensitive to the so-called resolved channels, while the direct channels contribute dominantly at large Q^2 . For small values of Q^2 , the kinematic reach is mainly limited by the forward acceptance of the scattered lepton, which removes substantial parts of the phase space where the cross-section from the resolved channels is large, thus motivating an enhanced forward-lepton coverage for precision studies of the photon structure.

In studies of lepton-proton scattering, the Breit frame is commonly used for jet studies. We observed that this is not suitable if a probe of resolved photon processes is aimed for. This is a consequence of the fact that in the Breit frame the Born-level leading jet is boosted into the current direction, hence impossible to be clustered. The direct channels are dominant for higher multiplicities and are thus enhanced in the Breit frame. In contrast, this is not the case in the laboratory frame, making it the preferred choice for jet measurements. In contrast, Breit-frame event shape observables that use the direction of the exchanged boson current as reference axis offer very much complementary information to jet cross sections. These event shapes measure the QCD activity along the current direction, and thus allow to probe the resolved photon process.

The main background to electron-photon scattering into jet final states is the production of W boson pairs, and we assess different cuts to reduce its contribution. We find that the best signal-to-background ratio is achieved by employing a cut on the jet multiplicity, $N \leq 1$, in the laboratory frame. However, the region of large Q^2 can not be fully separated from the background. In this region, sensitivity on the partonic content of the photon was already low due to the dominance of the direct process, and is further diminished due to the incomplete background separation.

Our work outlines the main aspects, opportunities and limitations of studying the partonic content of the photon through DIS-like jet production at future lepton colliders. More refined studies will require a more detailed modelling of the final state acceptance, once detector configurations have become mature.

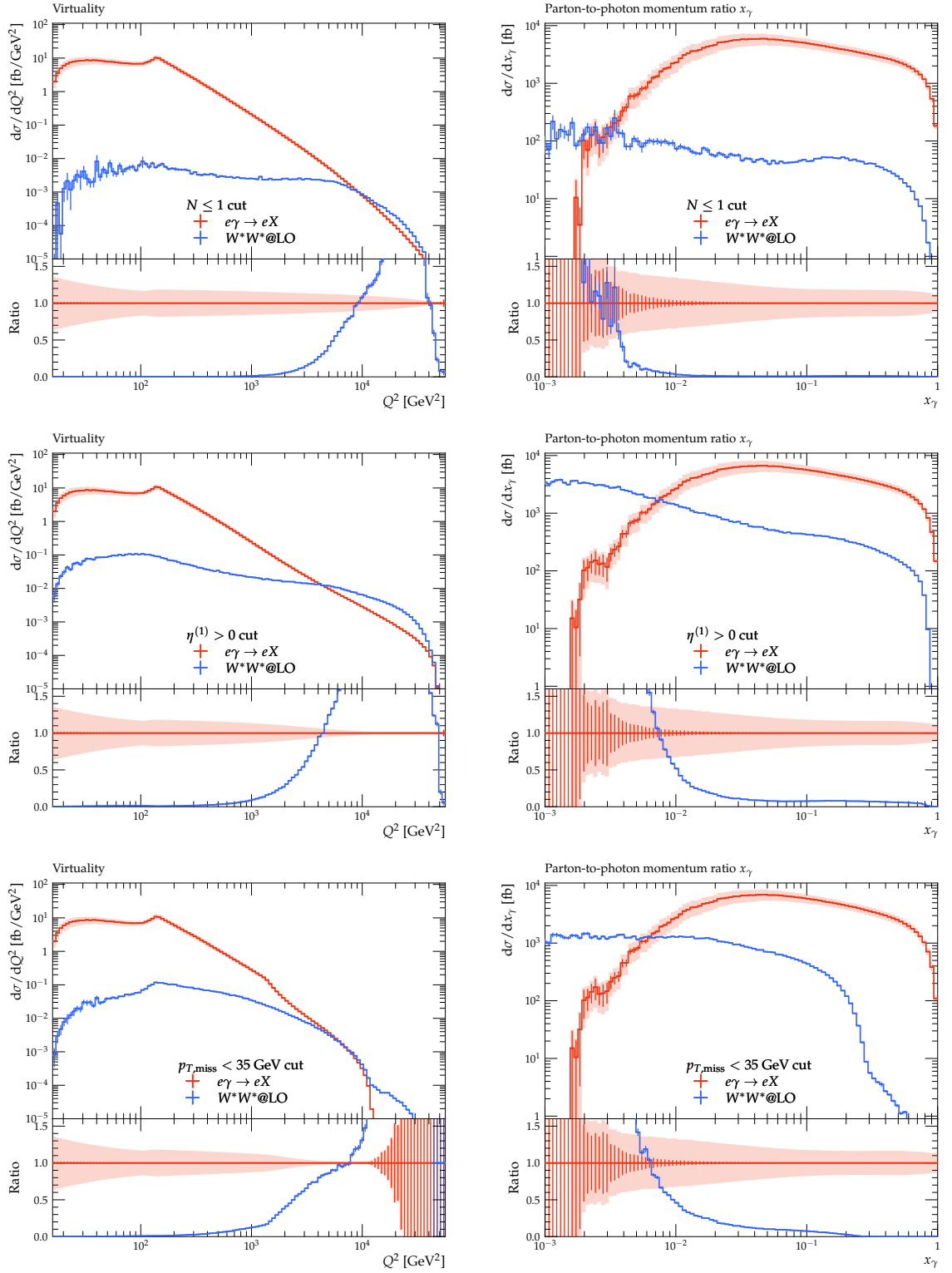


Figure 8: Distributions of virtuality Q^2 (left column) and Bjorken variable x_γ (right column) for $e\gamma \rightarrow eX$ and $e^+e^- \rightarrow W^*_{\rightarrow l\nu}W^*_{\rightarrow jj}$ with an additional cut on jet multiplicity $N = 1$ (top row), leading-jet pseudorapidity $\eta^{(1)} > 0$ (middle row) or missing transverse momentum $p_{T,\text{miss}} < 35$ GeV (bottom row).

Acknowledgments

PM thanks Stefan Höche for technical advice on the implementation. This work has been supported by the Swiss High Energy Physics initiative for the FCC (CHEF), with funding provided specifically by SERI and the University of Zurich, as well as by the Swiss National Science Foundation (SNF) under contract 240015.

References

- [1] T. F. Walsh and P. M. Zerwas, *Two photon processes in the parton model*, *Phys. Lett. B* **44** (1973) 195–198.
- [2] M. Klasen, *Theory of hard photoproduction*, *Rev. Mod. Phys.* **74** (2002) 1221–1282, [[hep-ph/0206169](#)].
- [3] E. Witten, *Anomalous Cross-Section for Photon-Photon Scattering in Gauge Theories*, *Nucl. Phys. B* **120** (1977) 189–202.
- [4] G. Altarelli and G. Parisi, *Asymptotic Freedom in Parton Language*, *Nucl. Phys. B* **126** (1977) 298–318.
- [5] Y. L. Dokshitzer, *Calculation of the Structure Functions for Deep Inelastic Scattering and e^+e^- Annihilation by Perturbation Theory in Quantum Chromodynamics.*, *Sov. Phys. JETP* **46** (1977) 641–653.
- [6] S. J. Brodsky, T. Kinoshita, and H. Terazawa, *Deep inelastic scattering of electrons on a photon target*, *Phys. Rev. Lett.* **27** (1971) 280–283.
- [7] P. M. Zerwas, *On Scaling in Inelastic Electron-Photon Scattering*, *Phys. Rev. D* **10** (1974) 1485.
- [8] M. Glück and E. Reya, *Boundary Conditions for the Photon Structure Function in the Leading and Subleading Order*, *Phys. Rev. D* **28** (1983) 2749.
- [9] **FCC Collaboration**, A. Abada et al., *FCC-ee: The Lepton Collider: Future Circular Collider Conceptual Design Report Volume 2*, *Eur. Phys. J. ST* **228** (2019) 261–623.
- [10] **CEPC Study Group** Collaboration, M. Dong et al., *CEPC Conceptual Design Report: Volume 2 - Physics & Detector*, [arXiv:1811.10545](#).
- [11] **ILC Collaboration**, H. Baer et al., *The International Linear Collider Technical Design Report - Volume 2: Physics*, [arXiv:1306.6352](#).
- [12] A. Accardi et al., *Electron Ion Collider: The Next QCD Frontier: Understanding the glue that binds us all*, *Eur. Phys. J. A* **52** (2016), no. 9 268, [[arXiv:1212.1701](#)].
- [13] M. Glück, E. Reya, and A. Vogt, *Photonic parton distributions*, *Phys. Rev. D* **46** (1992) 1973–1979.
- [14] H. Abramowicz, K. Charchula, and A. Levy, *Parametrization of parton distributions in the photon*, *Phys. Lett. B* **269** (1991) 458–464.

- [15] L. E. Gordon and J. K. Storrow, *The Parton distribution functions of the photon and the structure function $F_2^\gamma(x, Q^2)$* , *Z. Phys. C* **56** (1992) 307–314.
- [16] G. A. Schuler and T. Sjostrand, *Low and high mass components of the photon distribution functions*, *Z. Phys. C* **68** (1995) 607–624, [[hep-ph/9503384](#)].
- [17] M. Glück, E. Reya, and I. Schienbein, *Radiatively generated parton distributions of real and virtual photons*, *Phys. Rev. D* **60** (1999) 054019, [[hep-ph/9903337](#)]. [Erratum: *Phys.Rev.D* **62**, 019902 (2000)].
- [18] M. Krawczyk, A. Zembruski, and M. Staszel, *Survey of present data on photon structure functions and resolved photon processes*, *Phys. Rept.* **345** (2001) 265–450, [[hep-ph/0011083](#)].
- [19] **Sherpa** Collaboration, E. Bothmann et al., *Event generation with Sherpa 3*, *JHEP* **12** (2024) 156, [[arXiv:2410.22148](#)].
- [20] C. F. von Weizsacker, *Radiation emitted in collisions of very fast electrons*, *Z. Phys.* **88** (1934) 612–625.
- [21] E. J. Williams, *Nature of the high-energy particles of penetrating radiation and status of ionization and radiation formulae*, *Phys. Rev.* **45** (1934) 729–730.
- [22] V. M. Budnev, I. F. Ginzburg, G. V. Meledin, and V. G. Serbo, *The Two photon particle production mechanism. Physical problems. Applications. Equivalent photon approximation*, *Phys. Rept.* **15** (1975) 181–281.
- [23] S. Catani, F. Krauss, R. Kuhn, and B. R. Webber, *QCD matrix elements + parton showers*, *JHEP* **11** (2001) 063, [[hep-ph/0109231](#)].
- [24] S. Höche, F. Krauss, S. Schumann, and F. Siegert, *QCD matrix elements and truncated showers*, *JHEP* **05** (2009) 053, [[arXiv:0903.1219](#)].
- [25] T. Carli, T. Gehrmann, and S. Hoeche, *Hadronic final states in deep-inelastic scattering with Sherpa*, *Eur. Phys. J. C* **67** (2010) 73–97, [[arXiv:0912.3715](#)].
- [26] S. Hoeche, S. Schumann, and F. Siegert, *Hard photon production and matrix-element parton-shower merging*, *Phys. Rev. D* **81** (2010) 034026, [[arXiv:0912.3501](#)].
- [27] T. Gleisberg and S. Höche, *Comix, a new matrix element generator*, *JHEP* **12** (2008) 039, [[arXiv:0808.3674](#)].
- [28] S. Schumann and F. Krauss, *A Parton shower algorithm based on Catani-Seymour dipole factorisation*, *JHEP* **03** (2008) 038, [[arXiv:0709.1027](#)].
- [29] G. S. Chahal and F. Krauss, *Cluster Hadronisation in Sherpa*, *SciPost Phys.* **13** (2022), no. 2 019, [[arXiv:2203.11385](#)].
- [30] C. Bierlich, A. Buckley, J. M. Butterworth, C. Gutschow, L. Lönnblad, T. Procter, P. Richardson, and Y. Yeh, *Robust independent validation of experiment and theory: Rivet version 4 release note*, *SciPost Phys. Codeb.* **36** (2024) 1, [[arXiv:2404.15984](#)].
- [31] **H1** Collaboration, A. Aktas et al., *Measurement of event shape variables in deep-inelastic scattering at HERA*, *Eur. Phys. J. C* **46** (2006) 343–356, [[hep-ex/0512014](#)].